Discovery of a Huge Young Stellar Object Interaction Region in Camelopardalis

Ronald J. Buta – University of Alabama

et al.

Citation of published version:

McCall, M., et al. (2004): Discovery of a Huge Young Stellar Object Interaction Region in Camelopardalis. *The Astronomical Journal*, 128(1).
DOI: 10.1086/421370

The Astronomical Journal, 128:375–386, 2004 July

DISCOVERY OF A HUGE YOUNG STELLAR OBJECT INTERACTION REGION IN CAMELOPARDALIS

Marshall L. McCall,[1,2] Ronald J. Buta,[2,3] Tyler J. Foster,[4] Walter Huchtmeier,[5,6] and John Huchra[7,8]

Received 2003 June 30; accepted 2004 March 25

ABSTRACT

During the course of a wide-field *VI* survey of galaxies in the IC 342/Maffei Group, a large nebula, which looks like an inclined disk with a jetlike plume emerging from it, was discovered in Camelopardalis. The object is most prominent in *I*. The predominating disk component is 6.′8 across, which corresponds to 4.0 ± 1.6 pc at the estimated distance of 2.0 ± 0.8 kpc (the Perseus Arm). The plume extends 3.′8 (2.2 pc) outward from the core along a direction that is about 20° from the minor axis of the disk. The disk lies along the edge of a filament of dust and molecular gas in the Milky Way. The plume points toward the core of the filament. No large-scale emission is seen at Hα, and the nebula is invisible in Two Micron All Sky Survey (2MASS) images. About 30″ from the center of the disk is IRAS 04261+6339, which is a pair of unresolved Hα sources whose *IRAS* colors and spectra reveal them to be young stellar objects (YSOs). The northern of the two exhibits a near-infrared tail, which is 15″ (0.15 pc) long in *H* and directed 66° away from the plume. Although the stars are exposed, as in Class II YSOs, the spectral energy distribution of the pair rises beyond 2 μm, typical of Class I systems. It appears that they are transitional YSOs, with characteristics similar to those of Holoea (IRAS 05327+3404). The total brightness of the plume plus disk exceeds that of the stars by 1.6 mag in *I*, yet the $V-I$ color is bluer by only 0.50 mag. Thus, the nebula cannot be a consequence of reflection, even allowing for differential extinction. It is tentatively identified as a remnant of an outflow from a binary YSO, glowing from the photoluminescence of silicon nanoparticles.

Key words: dust, extinction — galaxies: general — galaxies: individual: UGCA 92 — infrared: general — stars: pre–main-sequence

1. INTRODUCTION

During the mid-1990s, two of the authors (M. L. M. and R. J. B.) carried out a Schmidt CCD survey of the IC 342–Maffei Group in order to measure accurate global photometric properties of member galaxies. Besides revealing the true extent of known heavily obscured galaxies, deep exposures in Cousins *I* proved to be particularly adept at locating additional objects previously unseen because of heavy obscuration (McCall & Buta 1995, 1997; McCall et al. 1995). This paper reports on another previously unrecognized source, believed to be Galactic, discovered while imaging the field of the dwarf irregular galaxy UGCA 92.

Images of UGCA 92 taken in Cousins *I* in 1995 revealed a large extended object 13′ to the northwest, which at first glance looked like a pair of interacting galaxies. However, no H I emission could be detected in extragalactic velocity windows. Also, IRAS 04261+6339 was found to be located near the center. This source had previously been revealed to be two stars in the Milky Way with spectra indicative of young stellar objects (YSOs) (Strauss et al. 1992). Given that the nebula was probably associated, further work was delayed by extragalactic priorities, although the object was discussed briefly by Buta & McCall (1999). Only the brightest portions are visible on the POSS-II,[9] which, in fact, were first noticed in 1996 by I. Karachentsev and V. Karachentseva (1996, private communication), and not even a hint of the nebula is visible on Two Micron All Sky Survey (2MASS)[10] images. Beyond IRAS 04261+6339, searches with NED,[11] SIMBAD,[12] VizieR (Ochsenbein et al. 2000), and the ADS[13] did not turn up any reference to an unusual source of any kind within 10′ of the center of the nebula. In particular, searches of the 87GB (Gregory & Condon 1991) and the 6CV (Hales et al. 1993) catalogs did not turn up any radio continuum sources. No pre–main-sequence stars or Herbig-Haro objects have been

[1] Department of Physics and Astronomy, York University, 4700 Keele Street, Toronto, ON M3J 1P3, Canada; mccall@yorku.ca.

[2] Visiting Astronomer, Kitt Peak National Observatory, National Optical Astronomy Observatory, which is operated by the Association of Universities for Research in Astronomy, Inc., under cooperative agreement with the National Science Foundation. Observations made with the Burrell Schmidt of the Warner and Swasey Observatory, Case Western Reserve University.

[3] Department of Physics and Astronomy, University of Alabama, Tuscaloosa, AL 35487-0324; buta@sarah.astr.ua.edu.

[4] Department of Physics, University of Alberta, Edmonton, AB T6G 2J1, Canada; now at Dominion Radio Astrophysical Observatory, Herzberg Institute of Astrophysics, National Research Council, P. O. Box 248, Penticton, BC V2A6k3, Canada; tyler.foster@nrc-cnrc.gc.ca.

[5] Max-Planck-Institut für Radioastronomie, Auf dem Hügel 69, Bonn 53121, Germany; huchtmeier@mpifr-bonn.mpg.de.

[6] Observations reported here were obtained with the 100 m telescope of the Max-Planck-Institut für Radioastronomie at Effelsberg.

[7] Harvard-Smithsonian Center for Astrophysics, 60 Garden Street, Cambridge, MA 02138; huchra@cfa.harvard.edu.

[8] Observations reported here were obtained at the MMT Observatory, a joint facility of the Smithsonian Institution and the University of Arizona.

[9] The Second Palomar Observatory Sky Survey (POSS-II) was made by the California Institute of Technology with funds from the National Science Foundation, the National Aeronautics and Space Administration, the National Geographic Society, the Sloan Foundation, the Samuel Oschin Foundation, and the Eastman Kodak Corporation. The Oschin Schmidt Telescope is operated by the California Institute of Technology and Palomar Observatory.

[10] This publication makes use of data products from the Two Micron All Sky Survey, which is a joint project of the University of Massachusetts and the Infrared Processing and Analysis Center/California Institute of Technology, funded by the National Aeronautics and Space Administration and the National Science Foundation.

[11] The NASA/IPAC Extragalactic Database (NED) is operated by the Jet Propulsion Laboratory, California Institute of Technology, under contract with the National Aeronautics and Space Administration.

[12] This research has made use of the SIMBAD database, operated at CDS, Strasbourg, France.

[13] This research has made use of NASA's Astrophysics Data System.

cataloged in this area either (Herbig & Bell 1988; Reipurth 1994). Given the precedent set by the International Astronomical Union (McCall et al. 1995), the object is referred to here by the name MB 4.

In § 2, observations of MB 4 and IRAS 04261+6339 are discussed. Reductions, including the removal of the myriads of foreground stars, are described in § 3. Morphology is analyzed in § 4. Measurements of the distance, extinction, dimensions, magnitudes, and colors for both nebula and stars are described in § 5. The nature of IRAS 04261+6339 and the origin of the nebula are discussed in § 6. Finally, conclusions are presented in § 7.

2. OBSERVATIONS

Optical images were acquired with the 0.6/0.9 m Burrell Schmidt telescope at Kitt Peak National Observatory in Tucson, Arizona. All images were acquired with a Tektronix 2048×2048 CCD camera, of which pixel sizes were 21 μm square. The CCD was fed an f/3.5 beam, so pixels subtended $2\farcs028$ and frames covered $69'$ on the sky. The readout noise was only 3 e^- pixel^{-1}, so exposures were sky-noise dominated.

Images were acquired in V (KPNO filter 1542, $\lambda_c = 5436$ Å, FWHM = 1004 Å), Cousins I (KPNO filter 1539, $\lambda_c = 8244$ Å, FWHM = 1954 Å), Hα (KPNO filter 1563, $\lambda_c = 6573$ Å, FWHM = 67 Å), and a continuum band adjacent to Hα (KPNO filter 1494, $\lambda_c = 6658$ Å, FWHM = 84 Å). Through each broadband filter, sequences of five or six 5 minute exposures were taken. The shortness of the exposures was motivated by the need to minimize the number of saturated stars in the very crowded fields under study. Because the magnification of the Schmidt changed somewhat with position in the field, the telescope pointing was fixed and autoguided throughout a sequence. Because of time limitations, only one exposure was possible in each narrowband filter.

Images centered on UGCA 92 were obtained first on the night of 1995 November 12 UT, with the total exposure being 25 minutes. The Moon was approaching third quarter, and faint cirrus was visible, although not in the direction of the galaxy. On noticing a possible new galaxy (MB 4), a confirming sequence totaling 15 minutes was performed with the telescope pointing adjusted by $20'$ to place the object on a different section of the CCD. Observations in V were made on the night of 1995 November 14, when the Moon was at third quarter. This night was photometric. Two sequences were taken, each of 30 minutes duration, with the telescope positioning adjusted by about $7'$ between them. The field was repeated in Cousins I during moonrise on the night of 1995 November 15, another photometric night, not only to confirm the existence of MB 4, but to ensure that an accurately calibrated image would be derivable. The exposure totaled 30 minutes. Finally, images in Hα and the adjacent continuum band were acquired on the night of 1995 November 16. The exposures were 15 minutes. The Moon was a waning crescent, and the sky was photometric.

Besides the usual calibration images, jittered 10 minute exposures of a "blank field" at relatively high Galactic latitude [α(B1950.0) = $01^h42^m15^s$, δ(B1950.0) = $14°07'41''$, $l = 141\fdg9$, $b = -46\fdg5$] were acquired after dark to facilitate flat-fielding. Six frames were acquired in Cousins I over two nights (November 12 and 15), and three in V on one night (November 14).

Spectra of the two stars at the position of IRAS 04261+6339 were acquired at the MMT on 1987 January 24 UT as part of a redshift survey. Exposure times were 180 and 240 s for the northern and southern component, respectively. Further details are provided by Strauss et al. (1992).

To evaluate whether or not MB 4 was extragalactic, a search for 21 cm radiation was carried out at Effelsberg on 1996 November 11. The velocity interval -500 to 3800 km s^{-1} was scanned in total-power mode. In addition, MB 4 was observed in frequency-switching mode on 1998 February 6, covering the velocity range -450 to 800 km s^{-1} at the center position and at four positions offset by an antenna beamwidth ($9\farcm3$) to the north, south, east, and west.

3. REDUCTIONS

Optical image reductions were carried out using IRAF.[14] Bias corrections were made using an overscan zone 32 columns wide in each image and a zero correction frame for each night constructed from the average of two sets of 11 bias frames acquired at the beginning and end of the night.

Considerable care was taken to ensure accurate flat fielding over the entire field of the CCD. Dome flat fields could not be used because it was not possible to employ exposures long enough to quench the shutter pattern while providing even illumination to the screen. Instead, twilight images acquired at the beginning of each night (when the Moon was below the horizon) were employed to remove pixel-to-pixel variations in response. All frames of the blank field acquired through each filter were combined to create an image suitable for removing low-frequency variations in response. Even though there were subtle variations from frame to frame in the I band, possibly due to airglow, experiments showed that the combination of all six images over two nights enabled excellent large-scale flattening of program fields, with an accuracy better than 0.5%. After completing basic corrections, images in each sequence were aligned and averaged.

To make surface photometry possible and to investigate morphology without the encumbrance of thousands of foreground stars, a sophisticated IRAF script KILLALL was developed to employ DAOPHOT to remove foreground stars. Essentially, 512×512 subsections of the images (with a border 40 pixels wide) were passed through ALLSTAR four times, and a final star-free image was constructed by piecing the processed sections back together. Residuals for each of the brighter unsaturated stars were then removed by interpolating a plane fitted to an encompassing annulus two pixels wide. Remaining faint stars were removed by running KILLALL once more with a lower detection threshold. Full details of the cleaning process are given in Buta & McCall (1999).

Both stellar and nebular photometry were calibrated using observations of Landolt standards (Landolt 1992). Details, including calibration equations, are given in Buta & McCall (1999). Standards were measured with PHOT using an aperture with a diameter of $14''$. Resulting zero-point uncertainties were 0.026 and 0.041 mag for November 14 (V) and November 15 (I), respectively.

Reductions of optical spectra are described by Strauss et al. (1992). Note that no effort was made to calibrate fluxes. Radio observations were reduced in the manner described by Huchtmeier et al. (1995).

4. MORPHOLOGY

Close-up views of MB 4 in Cousins I with and without foreground stars are given in Figure 1. The images displayed

[14] IRAF is distributed by the National Optical Astronomy Observatories, which is operated by the Association of Universities for Research in Astronomy, Inc., under contract to the National Science Foundation.

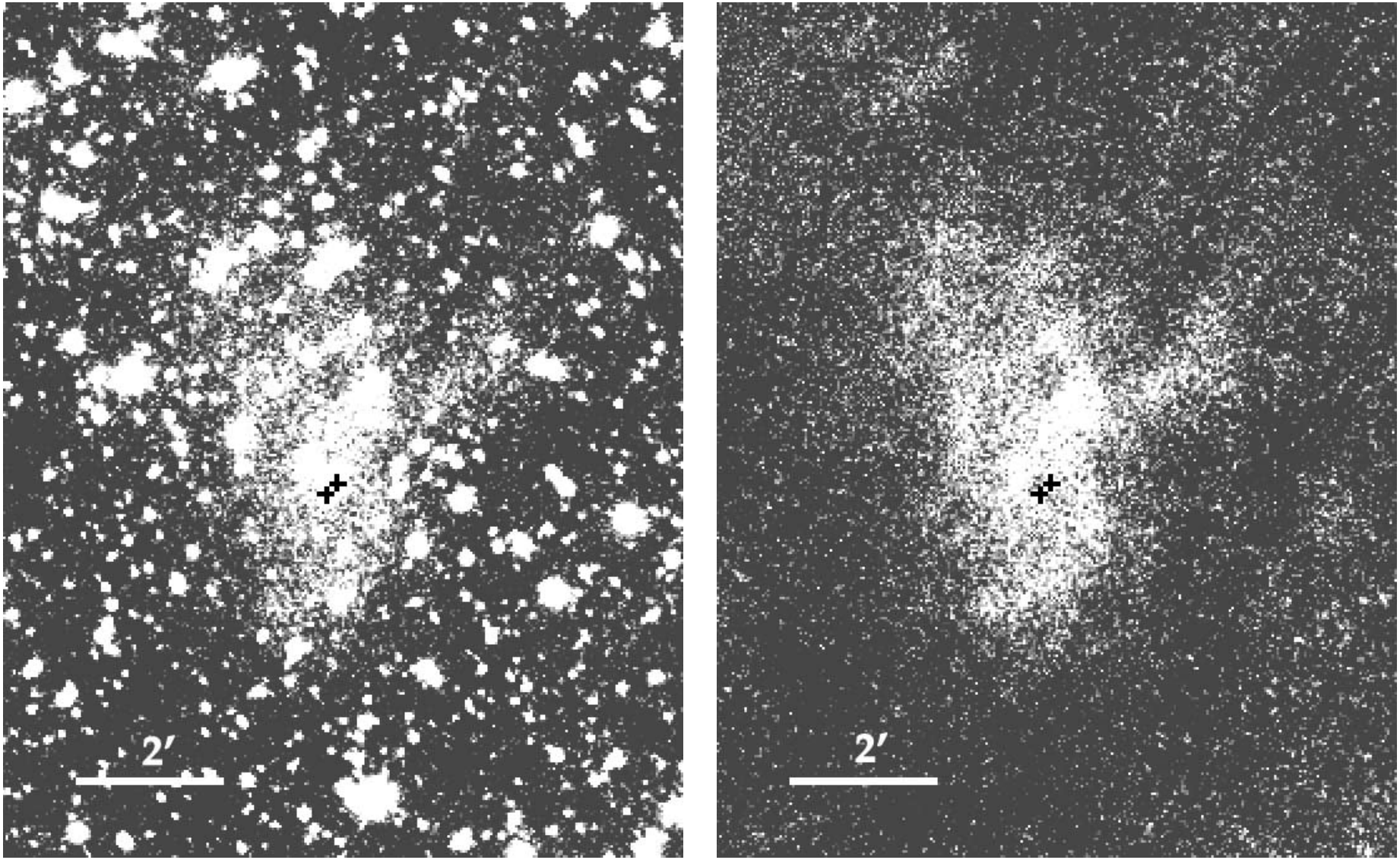

FIG. 1.—Close-ups of MB 4 in Cousins *I*. The left panel shows the field as it appears on the sky. In the right panel, foreground stars have been removed. The two images are displayed with the same brightness and contrast. Black crosses mark the positions of the optically visible components of IRAS 04261+6339, which are Hα sources. In both panels, north is up and east is to the left.

TABLE 1
POSITIONS

Source (1)	Classification (2)	α(1950) (3)	δ(1950) (4)	l (5)	b (6)	$\Delta\alpha$(B1950.0) (7)	$\Delta\delta$(B1950.0) (8)	r (9)
Hα North, in I	YSO	04 26 09.52	+63 39 30.2	144.497	+10.514	0.0 ± 0.7	0.0 ± 0.7	0.0
Hα South, in I	YSO	04 26 10.08	+63 39 25.4	144.498	+10.514	+3.7 ± 0.7	−4.8 ± 0.7	6.1
IRAS 04261+6339	Probably the YSOs	04 26 08.84	+63 39 28.6	144.496	+10.513	−4.5 ± 7.7	−1.6 ± 2.2	4.8
IRAS X0426+636	Probably the YSOs	04 26 12.0	+63 40 15	144.490	+10.526	+16.5 ± 111	+44.8 ± 111	47.8
MB 4 (centroid)	Stellar outflow?	04 26 10.8	+63 40 02	144.492	+10.522	+8.5 ± 7.6	+31.8 ± 14	32.9
UGCA 92	IBm	04 27 25.9	+63 30 22	144.708	+10.515	+508.4 ± 0.7	−548.2 ± 0.7	747.6

NOTE.—Col. (1): Name of object. Col. (2): Identification of object. If a galaxy, the revised Hubble type. Col. (3): Right ascension (B1950.0). Col. (4): Declination (B1950.0). Col. (5): Galactic longitude. Col. (6): Galactic latitude. Col. (7): Offset in right ascension from Hα North (positive eastward) along with the uncertainty in the right ascension of the object, both in arcseconds. Col. (8): Offset in declination from Hα North (positive northward) along with the uncertainty in the declination of the object, both in arcseconds. Col. (9): Angular distance from Hα North, in arcseconds.

are extracted from the average of the frames taken on November 15 and equate to a 30 minute exposure. The surface brightness of the faintest visible isophotes is about 26.5 mag arcsec^{-2}. Subtending 6.′8 on the sky, MB 4 is actually bigger than UGCA 92, the original target of the observations.

The images show a nebula that has the appearance of an inclined disk from which emerges a plume resembling a jet. The disk does not have a uniform surface brightness; in particular, there are enhancements to the south of the center and near the interface with the plume. The axis of the plume appears to be about 20° away from the minor axis of the disk. The end of the plume appears to be flared. Fundamental features are confirmed by the other shifted sequences of images described above. Henceforth, the words ''disk'' and ''plume'' are used to refer to the two distinct morphological components of MB 4 without regard to origins. It remains to be seen whether the first represents a physical structure with the geometry of a disk or if the second is, or was, associated with any movement of mass.

In V, MB 4 is extremely faint. Nevertheless, the morphology in V appears comparable to that in I. The continuum-subtracted Hα image shows two point sources near the center, which are coincident with two stars that are bright in I. However, no extended emission is visible, even though H II regions and diffuse emission are clearly detected in UGCA 92. At 21 cm, no emission above the rms noise of 8 mJy was detectable outside of the heliocentric velocity interval −140 to +20 km s^{-1}. Of course, there may be emission within that interval, but it cannot be recognized because of confusion with the Milky Way. On the POSS-II red image, patches of nebulosity are visible where the surface brightness is highest, namely near the center and the southern end of the disk, where the plume emerges from the disk, and perhaps at the end of the plume. However, no coherent structure is recognizable without prior knowledge of its existence. Hints of nebulosity are seen also on the blue image at the same locations. No nebulosity is seen around the Hα sources on either image. On 2MASS images, MB 4 is imperceptible.

Table 1 summarizes all relevant positions. Optical positions for MB 4, the two emission-line stars near the center, and UGCA 92 were measured from the six-frame average I-band image of November 15 using local software. A total of 24 positional standard stars from the Space Telescope Science Institute Guide Star Catalog was used for the analysis, yielding positions with a formal error of 0.″67. Note that the positions of the stars are consistent with those recorded in the Point Source Catalog of the 2MASS All-Sky Data Release (Cutri et al. 2003). The position given for MB 4 is the centroid of the disk component. The position of IRAS 04261+6339 is from the *IRAS* Faint Source Catalog (Moshir et al. 1990), and that of X0426+636 is from the *IRAS* Small-Scale Structure Catalog (Helou & Walker 1988).

The two emission-line stars, which are separated by 6.″1, are 33″ to the southwest of the center of the disk of MB 4. They appear to be half as far from the projected axis of the plume. Their positions are coincident with IRAS 04261+6339, which is visible as a pointlike source in all four *IRAS* wavebands in the co-added images of Field 393 in the *IRAS* Sky Survey Atlas Set II (see Wheelock et al. 1994). At 100 μm (at which the flux peaks), this source is slightly extended, so it is catalogued also as X0426+636 in the *IRAS* Small-Scale Structure Catalog (Helou & Walker 1988). However, that catalog's comparison of the 100 μm flux in the point source with that in the extended source suggests that the size of the extended source could be only 4.″3, which is comparable to the separation of the emission-line stars. It is also noted that the extended source might be the superposition of two close point sources. Overall, it appears that what *IRAS* detected was emission from the two point sources, not MB 4.

Although 2MASS did not detect extended emission, images from the All-Sky Data Release (Cutri et al. 2003) do reveal a ''tail'' emerging from the northern Hα source (the word ''tail'' is used to distinguish it from the feature seen on the larger scale; see also Magnier et al. 1996). Images in H and K_s are displayed in Figure 2. The tail appears sharpest in H. In J, only the base is visible. There is only marginal evidence for Hα emission at its location.

MB 4 is located at the end of a long filament of dust and gas. Figure 3 shows the *IRAS* view of the region at 100 μm with sampling of 1.′5 pixel^{-1} (see Wheelock et al. 1994), as provided by Skyview[15] (McGlynn et al. 1998). Superimposed are 2.6 mm ^{12}CO contours derived from a composite of many surveys sampled at 7.′5 pixel^{-1} (Dame et al. 2001). The stick figure drawn to the upper right of center is a magnified depiction of MB 4. It displays the relative sizes and orientations of the disk and plume. The longer bar, which marks the disk, is centered on IRAS 04261+6339. The disk lies along the edge of the filament, while the plume protrudes into the filament in a direction close to that of the maximum gradient in density. Note that there is no hint of MB 4 in the CO map.

[15] We acknowledge the use of NASA's SkyView facility (http://skyview.gsfc.nasa.gov) located at NASA Goddard Space Flight Center.

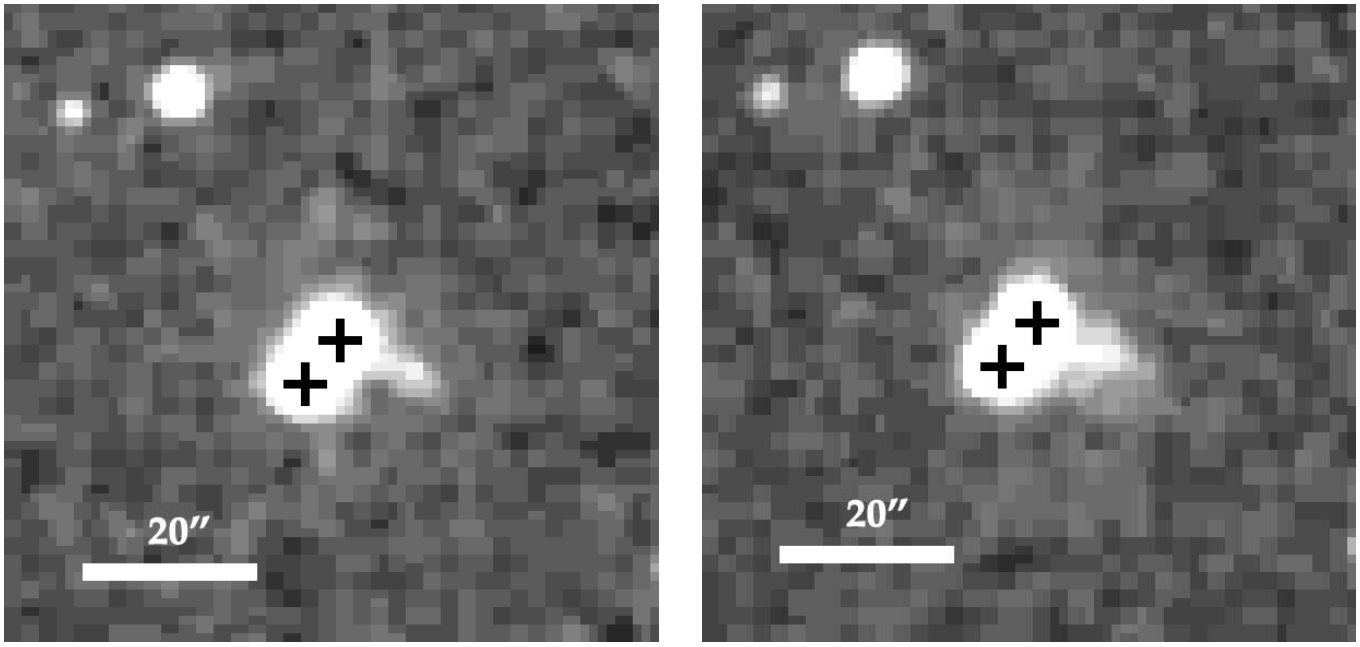

FIG. 2.—2MASS views (*left*, *H*; *right*, K_s) of the two Hα sources near the center of MB 4 (IRAS 04261+6339). In both panels, north is up and east is to the left. Black crosses mark the pixels with maximum intensity. Note the tail emerging from the northern component.

Infrared colors for IRAS 04261+6339 can be used to evaluate whether the stars are in an early or late stage of evolution (Ivezić & Elitzur 2000). *IRAS* fluxes are well determined (qualities range from 2 to 3), with $\log [F_\nu(12\ \mu\mathrm{m})/F_\nu(25\ \mu\mathrm{m})] = -0.56 \pm 0.03$ and $\log [F_\nu(60\ \mu\mathrm{m})/F_\nu(100\ \mu\mathrm{m})] = -0.39 \pm 0.03$. Thus, using the terminology of Ivezić & Elitzur (2000), the system is unquestionably a source of Class D, ruling out any possibility that it is a pair of AGB stars (see also Kwok 2000). The vast majority of such sources are young (Ivezić & Elitzur 2000). Spectra of each stellar component of IRAS 04261+6339 are displayed in Figure 4. Both show strong Hα emission, and the northern component also shows Ca II H and K in emission, as is characteristic of protostars. Velocities are consistent with placement in the Perseus Arm (§ 5.1). Considering also the coincidence in position with a well-defined cloud of dust and gas, we conclude that IRAS 04261+6339 is a pair of YSOs.

It is common for YSOs to be found in regions where there is nebulosity on large scales (Hodapp 1994; Magnier

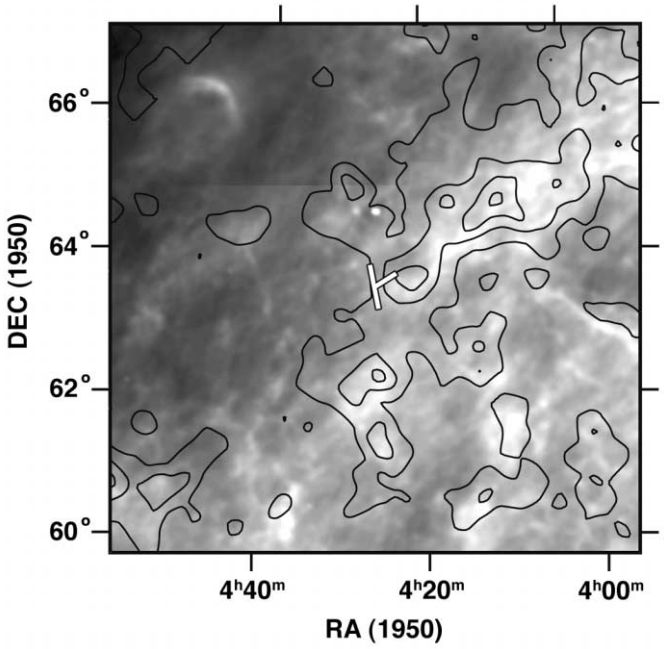

FIG. 3.—Image of the sky around MB 4 as seen by *IRAS* at 100 μm. Contours delineate ^{12}CO emission. The velocity-integrated main-beam brightness temperature for the contours ranges from 4 to 16 K km s^{-1} in steps of 4 K km s^{-1}. MB 4 is indicated by the white stick figure, the components of which give the orientations and sizes (grossly amplified) of the disk and plume. The longer bar, which marks the disk, is centered on IRAS 04261+6339. MB 4 is at the edge of a filament of dust and gas.

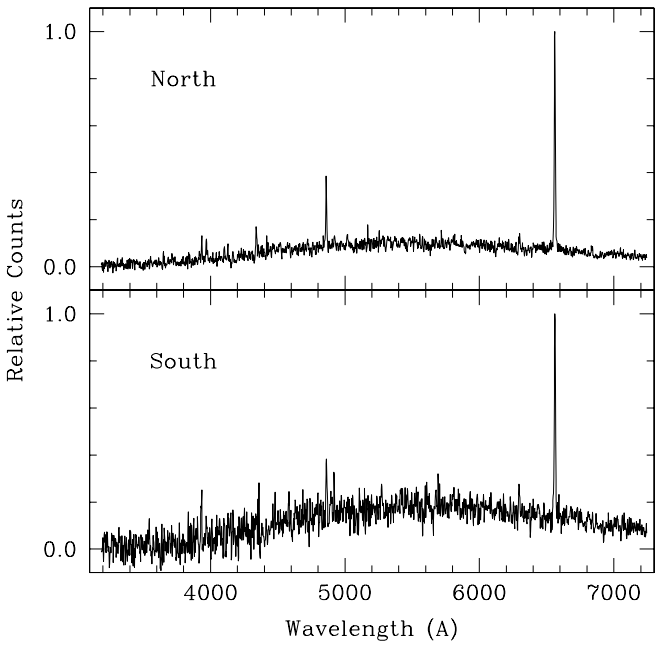

FIG. 4.—Spectra of the two optically visible components of IRAS 04261+6339. Neither has been flux calibrated. Ca II emission is obvious in the northern component.

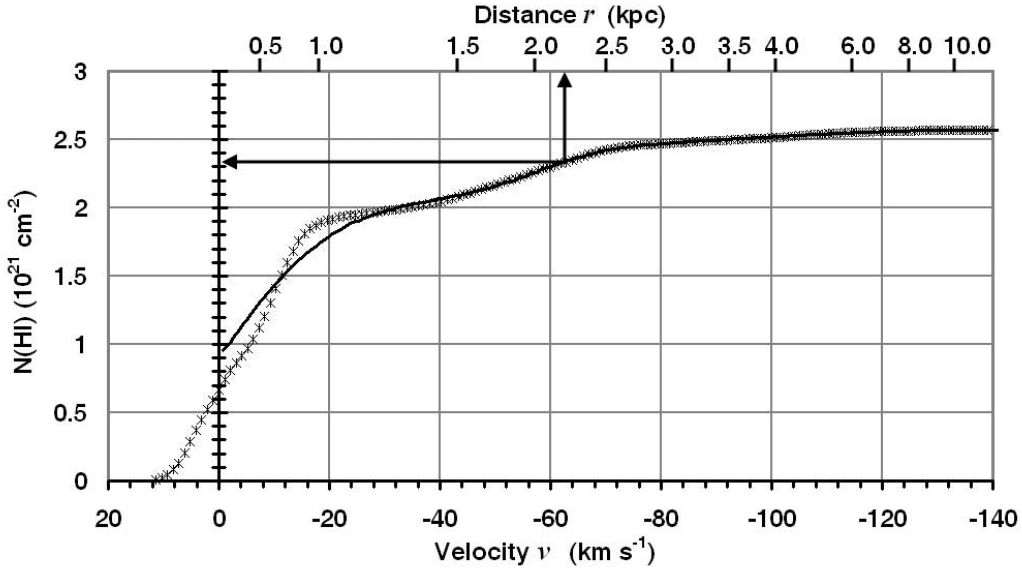

FIG. 5.—Cumulative H I column density vs. velocity toward $l = 144.^{\circ}5$, $b = 10^{\circ}$. Crosses are observations from the Leiden-Dwingeloo H I survey (Burton & Hartmann 1994), while the solid line is the fit derived via the technique of Foster & Routledge (2002). H I at positive velocities (forbidden by circular rotation) was given zero weighting in the fitting process. The quality of the fit out to 10 kpc is $\chi^2/\nu \sim 1$, but the uncertainties in the velocity-distance relation are increasingly large beyond about 4 kpc in this direction. The mean column density (2.35×10^{21} cm^{-2}) and corresponding distance (2.2 kpc) to IRAS 04261+6339 are marked with arrows.

et al. 1999b), so it is logical to associate MB 4 with IRAS 04261+6339. What makes MB 4 special is its large-scale coherence. Most nebulosity around YSOs is chaotic, except for a few systems that have elements akin to bow shocks. Coherent structures are normally seen only on very small scales, like that of the tail of IRAS 04261+6339. It may be significant that the selection process was opposite to that which normally accompanies analyses of YSOs. The nebulosity was discovered first, and the morphology in turn guided investigations toward IRAS 04261+6339, rather than the other way around.

If MB 4 were extragalactic, it would have to be either an interacting pair of galaxies or an active galaxy with an optically visible jet. If so, the morphology of the disk component would imply that there is a late-type galaxy in the system, which ought to be bright in Hα and at 21 cm. Although it is possible that the object is so near that its 21 cm emission is confused with emission from the Milky Way (between -140 and +20 km s^{-1} heliocentric), the lack of Hα emission suggests that the extragalactic interpretation is untenable.

5. MEASUREMENTS

5.1. *Distance*

At the moment, the only way of judging the extinction and distance of MB 4 is through the velocities of the two components of IRAS 04261+6339. The spectra shown in Figure 4 give heliocentric velocities of -91 ± 43 and -52 ± 48 km s^{-1} for the northern and southern YSO, respectively. Within errors, the two velocities are consistent, although it is certainly possible that there is some difference due to orbital motion. The unweighted mean, -71.5 km s^{-1}, is adopted as the systemic velocity. The mean error, 32 km s^{-1}, is adopted as the uncertainty. The *I*-band luminosity-weighted mean, which might be more indicative of the systemic velocity if luminosity traces mass, is almost the same as the unweighted mean, namely -75 km s^{-1}.

For objects in the second quadrant with high line-of-sight velocities, kinematic distances predicted by a flat rotation curve tend to be excessively large (Foster & Routledge 2002). For example, with $R_{\odot} = 8.0$ kpc and $v_{\odot} = 220$ km s^{-1}, the distance of IRAS 04261+6339 from the Sun comes out to be 11 kpc, which can be dismissed as unreasonable. Foster & Routledge (2002) propose a new method that yields significantly improved distance estimates from velocities. This method is applied here.

Foster & Routledge (2002) principally assume that, on a large scale, the observed line-of-sight velocity for atomic hydrogen emission becomes increasingly negative with distance. Although small velocity reversals (e.g., shocked H I in expanding shells or in the spiral arms) may exist along the line of sight, the material responsible is generally not seen in emission, because the H I is compressed into dense optically thick features. On a large scale, for H I in emission and in circular rotation, the assumption that distance varies monotonically with velocity is fundamentally correct.

Foster & Routledge (2002) begin with a model of the integrated H I column density versus distance, $N(\mathrm{H\ I})(r)$. It is linked to velocity space via a velocity-to-distance mapping function $v(r)$. Parameters of both the model $N(\mathrm{H\ I})(r)$ and the mapping function $v(r)$ are determined by fitting the observed $N(\mathrm{H\ I})(v)$. Convergence is achieved by χ^2 minimization. The approach yields both the model $N(\mathrm{H\ I})(r)$ and the function $v(r)$ that best reproduces the observed distribution $N(\mathrm{H\ I})(v)$.

Figure 5 shows how the cumulative H I emission column density $N(\mathrm{H\ I})$ varies with the line-of-sight velocity v in the direction of IRAS 04261+6339 (actually, $l = 144.^{\circ}5$, $b = 10^{\circ}$). Observations are extracted from the Leiden-Dwingeloo survey (Burton & Hartmann 1994). Based on the measured velocities, the integrated H I column densities to the northern and southern component of IRAS 04261+6339 are $(2.2 \pm 0.8)10^{21}$ and $(2.5 \pm 0.2)10^{21}$ cm^{-2}, respectively. The unweighted mean column density, $(2.35 \pm 0.41)10^{21}$ cm^{-2}, is adopted for estimating the distance.

The solid curve in Figure 5 gives the fit to $N(\mathrm{H\ I})(v)$. The adopted distance to the Galactic center is 8.0 kpc (Reid 1993). The model places the center of the Perseus Arm at a distance

of 2.0 ± 0.8 kpc, where the uncertainty is the 3 σ half-width found for the arm. The mean distance derived for the pair of stars associated with IRAS 04261+6339 is 2.2 ± 1.1 kpc. The bulk of the error in the distance comes from the uncertainty in the integrated column density (i.e., the uncertainty in the mean velocity of the YSOs), with only 0.25 kpc contributed by intrinsic uncertainty in the model of $N(\mathrm{H\ I})(r)$. Although the uncertainty is large, it appears likely that the stars are residents of the Perseus Arm. Here, then, the distance of the Perseus Arm, 2.0 ± 0.8 kpc for $R_\odot = 8.0$ kpc, is adopted as the distance to IRAS 04261+6339 and, by association, MB 4.

5.2. *Extinction*

The Galactic extinction toward IRAS 04261+6339 can be estimated from the column density of hydrogen. From *Copernicus* satellite observations of O and B stars, Bohlin et al. (1978) found

$$\frac{N(\mathrm{H\ I}) + N(\mathrm{H\ II}) + 2N(\mathrm{H_2})}{E(B-V)} = (6.0 \pm 0.35) \times 10^{21}\ \mathrm{cm^{-2}\ mag^{-1}}.$$

Based on the H I model derived in § 5.1, the column density of neutral hydrogen toward IRAS 04261+6339 is $(2.25 \pm 0.25)10^{21}$ cm^{-2} if the object is located in the middle of the Perseus Arm. The average integrated brightness temperature of ^{12}CO emission in this direction is (5.35 ± 1.3) K km s^{-1} (Dame et al. 2001). The emission probably comes predominantly from material nearer than IRAS 04261+6339, because the CO profile toward $l = 144.^\circ5$, $b = 9.^\circ5$ in the older Columbia survey only shows two 5 σ peaks near 0 km s^{-1} and one 3 σ peak at -55 km s^{-1} (Dame et al. 1987). The Galactic longitude is well away from the anticenter, and the Galactic latitude is high, so it is likely that much of the emission is unsaturated. Thus, based on the CO-to-H_2 conversion factor derived from the distribution of diffuse γ-ray emission in the Milky Way (Strong & Mattox 1996), the column density of H_2 is estimated to be $(1.02 \pm 0.27)10^{21}$ cm^{-2}. Assuming that there is a negligible amount of ionized hydrogen along the line of sight, then the color excess $E(B-V)$ due to Galactic dust must be 0.71 ± 0.11.

Because of shifts in effective wavelengths, the value of a color excess depends on the shape of the spectral energy distribution (SED) of the probe. To quantify extinction in a manner independent of SEDs, McCall & Armour (2000) and McCall (2004) recommend evaluating the optical depth at 1 μm. Knowledge of the optical depth at a fiducial wavelength then allows computation of the extinction of any SED in any bandpass. Here, it is presumed that the color excess derived from the column density of hydrogen is a consequence of obscuration by dust in the diffuse component of the interstellar medium. Therefore, the appropriate value of the ratio of total to selective extinction to adopt for an A0 V SED is $R_V = A_V/E(B-V) = 3.07 \pm 0.05$ (see McCall & Armour 2000). The reddening law of Fitzpatrick (1999), appropriately tuned to give $R_V = 3.07$ for Vega, is adopted as representative of the diffuse interstellar medium. Assuming that the value of $E(B-V)$ derived for IRAS 04261+6339 is indicative of what would be observed for a B0 V star at the same location [given how $N(\mathrm{H})/E(B-V)$ was defined], then the optical depth at 1 μm is $\tau_1 = 0.739 \pm 0.116$.

After correction for galactic extinction, the optical/near-infrared colors of the stars in IRAS 04261+6339 match reasonably well those of an unobscured M1 giant (see § 6.1). Therefore, values of extinction coefficients for bandpasses for which photometric data are available have been derived from the adopted reddening law by integrating response curves over the SED of an M1 III star (Pickles 1998) shifted by -72 km s^{-1} and extinguished by Galactic dust with $\tau_1 = 0.739$. Results for the Galactic extinction are summarized in Table 2.

TABLE 2

Integrated Properties of the YSOs in MB 4 and Holoea

Parameter	MB 4[a]	Holoea[b]
(1) Distance (kpc)	2.00 ± 0.80[c]	1.33 ± 0.12[d]
(2) Distance modulus (mag)	11.51 ± 0.87	10.62 ± 0.20
(3) $E(B-V)$ (Type = B V)	0.71 ± 0.11	0.25 ± 0.02
(4) τ_1	0.739 ± 0.116	0.264 ± 0.021
(5) A_V	2.047 ± 0.321	0.729 ± 0.058
(6) A_I	1.162 ± 0.182	0.415 ± 0.033
(7) A_J	0.557 ± 0.087	0.199 ± 0.016
(8) A_H	0.357 ± 0.056	0.128 ± 0.010
(9) A_{Ks}	0.242 ± 0.038	0.087 ± 0.007
(10) M_V	2.48 ± 0.93	7.39 ± 0.21
(11) $(V-I)^0$	1.75 ± 0.15	2.07 ± 0.06
(12) $(V-J)^0$	3.19 ± 0.24	4.64 ± 0.07
(13) $(V-H)^0$	4.19 ± 0.27	5.45 ± 0.08
(14) $(V-K_s)^0$	4.85 ± 0.29	6.39 ± 0.09
(15) $\log L_{25}$	15.06 ± 0.35	14.74 ± 0.10
(16) $m_{12}-m_{25}$	1.39 ± 0.08	1.19 ± 0.23
(17) $m_{25}-m_{60}$	1.51 ± 0.08	1.53 ± 0.23
(18) $m_{25}-m_{100}$	2.48 ± 0.08	1.97 ± 0.23
(19) Tail length (arcsec)	15.5 ± 1.2	23.5 ± 1.6
(20) Tail length (pc)	0.15 ± 0.06	0.15 ± 0.02
(21) Tail position angle (deg)	-123 ± 2	22 ± 8

Note.—Row (1): Distance in kpc. Row (2): Distance modulus in magnitudes. Row (3): Color excess due to Galactic dust for an SED (Pickles 1998) with spectral type B V (B0 V for MB 4, B5–7 V for Holoea). Row (4): Optical depth at 1 μm due to Galactic dust. Rows (5)–(9): Galactic extinctions in V, I, J, H, and K_s, derived from the optical depth at 1 μm. In the case of MB 4, these were computed from extinction coefficients for a SED with type M1 III extinguished only by Galactic dust with the optical depth given in row 4. In the case of Holoea, these were computed from extinction coefficients for a SED with type K2 III extinguished by dust in its immediate vicinity with an optical depth of 0.72 at 1 μm and by Galactic dust with the optical depth given in row 4. Row (10): Total absolute magnitude in V (2 stars in the case of MB 4, 1 star in the case of Holoea), corrected for Galactic extinction. Rows (11)–(14): Total colors, corrected for Galactic reddening. Row (15): Logarithm of the luminosity per unit frequency at 25 μm, in W Hz^{-1}. Row (16): $-2.5 \log F_\nu[(12\ \mu\mathrm{m})/F_\nu(25\ \mu\mathrm{m})]$. Row (17): $-2.5 \log F_\nu[(25\ \mu\mathrm{m})/F_\nu(60\ \mu\mathrm{m})]$. Row (18): $-2.5 \log F_\nu[(25\ \mu\mathrm{m})/F_\nu(100\ \mu\mathrm{m})]$. Row (19): Length of tail in H in arcseconds. Row (20): Length of tail in H in pc. Row (21): Position angle of tail in H, in degrees east of north.

[a] Data from 12 to 100 μm are for IRAS 04261+6339.

[b] Data from 12 to 100 μm are for IRAS 05327+3404. Optical and near-infrared magnitudes exclude the tail.

[c] Perseus Arm, assuming $R_\odot = 8.0 \pm 0.5$ kpc (Reid 1993).

[d] M36 (Sanner et al. 2000), based on A_V/τ_1 for the F8 V SED of Pickles (1998).

5.3. *Magnitudes and Colors*

Magnitudes of the YSOs in the field of MB 4 were derived by fitting a point-spread function (PSF) with a diameter of 8.″1. To determine the corrections needed to bring the photometry onto the Landolt system, growth curves were constructed for uncrowded stars. The aperture corrections required amounted to 0.13 and 0.18 mag in V and I, respectively.

Photometry of each YSO is presented in Table 3. Photometric parameters for the combined light of the two YSOs are given in Table 2. Near-infrared magnitudes are from the Point

TABLE 3
INDIVIDUAL PROPERTIES OF THE YSOs IN MB 4

Parameter[a]	North	South
(1) $v_\odot$ (km s^{-1})	-91 ± 43	-52 ± 48
(2) V	16.573 ± 0.023	17.055 ± 0.023
(3) I	13.959 ± 0.045	14.389 ± 0.015
(4) $V-I$	2.614 ± 0.051	2.666 ± 0.027
(5) $V-J$	4.590 ± 0.044	4.798 ± 0.030
(6) $V-H$	5.726 ± 0.054	6.082 ± 0.030
(7) $V-K_s$	6.480 ± 0.050	6.880 ± 0.031
(8) V^0	14.53 ± 0.32	15.01 ± 0.32
(9) $(V-I)^0$	1.73 ± 0.15	1.78 ± 0.14
(10) $(V-J)^0$	3.10 ± 0.24	3.31 ± 0.24
(11) $(V-H)^0$	4.04 ± 0.27	4.39 ± 0.27
(12) $(V-K_s)^0$	4.68 ± 0.29	5.08 ± 0.29
(13) M_V	3.02 ± 0.93	3.50 ± 0.93

NOTE.—Row (1): Heliocentric radial velocity. Row (2): Apparent magnitude in V. Row (3): Apparent magnitude in I. Rows (4)–(7): Apparent colors. Row (8): Apparent magnitude in V, corrected for extinction. Rows (9)–(12): Colors, corrected for reddening. Row (13): Absolute magnitude in V, assuming a distance of 2.00 ± 0.80 kpc.

[a] In this table only, errors in photometric zero points are not included in tabulated uncertainties for photometric quantities. In V, the zero-point error is 0.026 mag, and in I it is 0.041 mag.

Source Catalog of the 2MASS All-Sky Data Release (Cutri et al. 2003), and far-infrared fluxes are from the *IRAS* Faint Source Catalog (Moshir et al. 1990). Also provided in Table 2 are the length and orientation of the tail associated with the northern component, from the H-band image of the 2MASS All-Sky Data Release.

Surface photometry of the nebula in V and I was carried out using the star-free versions of the combined images of November 14 and 15, respectively. GALPHOT (from W. Freudling at European Southern Observatory) was used to quantify the center and orientation of the system, and local software was employed to do the photometry. Full details are given by Buta & McCall (1999).

Isophotes of MB 4 could be detected down to 27.8 mag arcsec^{-2} in V and 26.5 mag arcsec^{-2} in I. To determine total magnitudes, the surface brightness profile at large radii was modeled with an exponential, the parameters for which were used to extrapolate to infinity. Additional measurements of the dimensions and orientation of various features were made from the I-band image after 4×4 block-averaging.

Table 4 gives measured and derived parameters for MB 4. All corrections for Galactic extinction were taken from Table 2. Angular measures were converted to physical lengths using a distance of 2.0 ± 0.8 kpc.

6. DISCUSSION

6.1. *The Stars*

The apparent association of MB 4 with IRAS 04261+6339 suggests that it is somehow related to the evolution of a young stellar object. In the nomenclature of Lada (1988), a Class I YSO is a system that displays a SED that rises beyond 2 μm, but in which the source of radiation is so heavily obscured that it is invisible. A Class II system is one in which the SED is flat or falling in the infrared and in which the central source is readily observable, usually as a T Tauri star.

Class I systems are attributed to protostars that are still accreting material from their surroundings. A wealth of data on associated nebulae suggests that the geometry of the gas and dust is disklike and that the accretion is accompanied by mass ejections out of the poles. Eventually, a Class I system is believed to turn into a Class II system after undergoing a transition that leads to the dispersal of surrounding gas and dust and exposure of the protostar.

IRAS 04261+6339 shares properties of both Class I and Class II systems. The spectral energy distribution steadily rises beyond 2 μm (see Fig. 6), but the source of radiation is optically exposed. Indeed, it is similar to IRAS 05327+3404 (Holoea), which Magnier et al. (1999a) has identified as a transition object with *IRAS* colors like those of FU Orionis stars.

Magnier et al. (1999b) define a YSO in transition to be an *IRAS* source with

$$0.40 < -2.5 \log F_{12}/F_{25} < 1.3,$$
$$1.0 < -2.5 \log F_{25}/F_{60} < 2.0.$$

Subscripts refer to the wavelengths of the *IRAS* bandpasses in μm. The middle of the first window is the color of a flat source, while that of the second is the color of Holoea. The breadths of the windows are set by the 2 σ dispersion observed in each color.

TABLE 4
PROPERTIES OF MB 4

Whole		Disk		Plume	
Parameter	Value	Parameter	Value	Parameter	Value
(1) V	13.97 ± 0.11	(7) f_V	~ 0.83	(14) f_V	~ 0.17
(2) I	11.83 ± 0.17	(8) f_I	~ 0.84	(15) f_I	~ 0.16
(3) $V-I$	2.14 ± 0.21	(9) Position Angle (deg)	10.8 ± 1.1	(16) Position Angle (deg)	-57.2 ± 3.3
(4) V^0	11.92 ± 0.34	(10) Axis ratio (inner)	0.37 ± 0.03	(17) Length (arcmin)	3.81 ± 0.14
(5) $(V-I)^0$	1.26 ± 0.25	(11) Axis ratio (outer)	0.59 ± 0.06	(18) Length (pc)	2.22 ± 0.89
(6) M_V	0.42 ± 0.93	(12) Major axis (arcmin)	6.80 ± 0.54	(19) Width before flare (arcmin)	1.45 ± 0.27
		(13) Major axis (pc)	4.0 ± 1.6	(20) Width before flare (pc)	0.84 ± 0.37

NOTE.—Row (1): Apparent magnitude in V. Row (2): Apparent magnitude in I. Row (3): Apparent $V-I$ color. Row (4): Apparent magnitude in V corrected for extinction. Row (5): Apparent $V-I$ color corrected for reddening. Row (6): Absolute magnitude in V. Row (7): Fraction of total light in V. Row (8): Fraction of total light in I. Row (9): Position angle of major axis in I, in degrees (1950). Row (10): Axis ratio of inner isophotes in I (minor relative to major). Row (11): Axis ratio of outer isophotes in I (minor relative to major). Row (12): Length of major axis in I (arcmin). Row (13): Length of major axis in I (pc). Row (14): Fraction of total light in V. Row (15): Fraction of total light in I. Row (16): Position angle in I in degrees (1950). Row (17): Length measured from center of disk to end of flare in I (arcmin). Row (18): Length measured from center of disk to end of flare in I (pc). Row (19): Maximum width before flare in I (arcmin). Row (20): Maximum width before flare in I (pc).

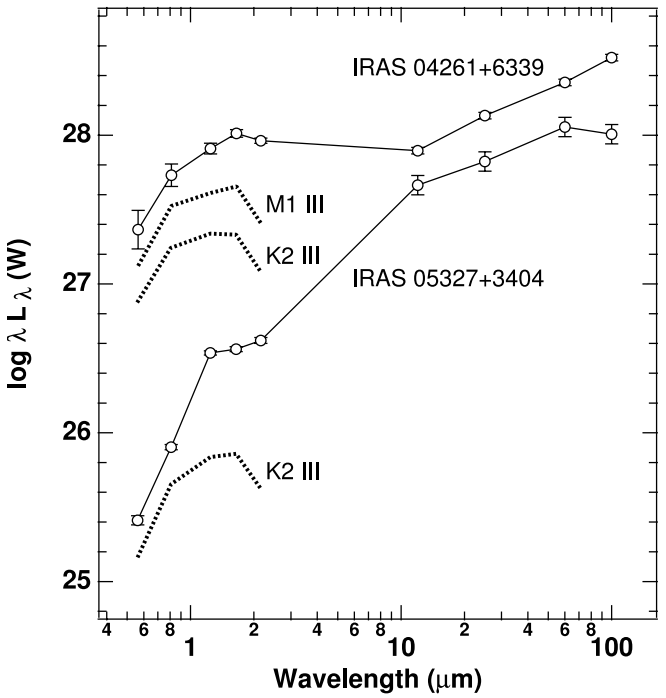

FIG. 6.—Absolute SEDs for the YSOs in MB 4 and Holoea, corrected for Galactic extinction only. Dotted curves below the SED for IRAS 04261+6339 show broadband SEDs for an unobscured M1 giant and for a K2 giant reddened locally by normal dust with an optical depth of 0.46 at 1 μm. The dotted curve below the SED for IRAS 05327+3404 shows the broadband SED for a K2 giant reddened locally by normal dust with an optical depth of 0.72 at 1 μm. The SEDs for the giants are placed arbitrarily.

IRAS colors for MB 4 and Holoea are given in Table 2. No corrections for reddening have been applied. MB 4 falls just outside of the first window but is right in the middle of the second. Considering uncertainties, both colors are consistent with those of Holoea. Thus, the YSOs of MB 4 can be considered to be a pair in transition.

Holoea is superimposed on the star cluster M36, although it remains uncertain as to whether or not it is associated. It may be an outlying member of S235, which is at a comparable distance but 2° away. Probably the best estimates of the distance and foreground reddening of Holoea come from the color-magnitude diagram of M36, which has been measured recently by Sanner et al. (2000). The derived color excess, $E(B-V) = 0.25 \pm 0.02$, is predominantly based on the colors of the early-type stars in the color-magnitude diagram. Adopting the B5–7 V SED of Pickles (1998) as representative of these stars, then the color excess implies that the optical depth at 1 μm due to Galactic dust is $\tau_1 = 0.264 \pm 0.021$.

The average spectral type of the stars setting the apparent distance modulus of M36 (11.375 in V) can be considered to be F8 V. Thus, based on the Galactic value of τ_1, the appropriate value of the extinction to use to correct the distance modulus is $A_V = 0.75 \pm 0.06$, which leads to a distance for Holoea of 1.33 ± 0.12 kpc.

Based on deep spectroscopy, the YSO in Holoea has a spectral type around K2 III (Magnier et al. 1999a). To match the optical portion of the SED, however, it is necessary that such a star be obscured significantly by dust in its immediate vicinity (see Magnier et al. 1999a). After correcting for the foreground dust, $E(V-I)$ implies that the optical depth at 1 μm of localized dust must be $\tau_1 = 0.72$. Thus, extinction coefficients for the YSO for relevant bandpasses were computed using the SED for a K2 III star (Pickles 1998) at rest, obscured locally by dust with $\tau_1 = 0.72$ and extinguished by Galactic dust with $\tau_1 = 0.264$. The resulting estimates of the Galactic component of the extinction are given in Table 2.

Derived integrated properties of the YSOs in MB 4 and Holoea are compared in Table 2, and spectral energy distributions are compared in Figure 6. Only corrections for *Galactic* extinction have been applied. Also displayed in the figure are broadband SEDs for selected giants (see below). Colors for the giants were derived by integrating spectra of Pickles (1998) after weighting them by system response curves for V, I, J, H, and K_s provided by Bessell (1990) and Wheaton (2000). Note that the photometry presented for MB 4 refers to the combined light of the two YSOs there, as judged from the data given in Table 3. All photometry for Holoea is taken from Magnier et al. (1999a), near-infrared magnitudes having been converted to the 2MASS system via the transformation equations of Hawarden et al. (2001) and Carpenter (2001). Uncertainties in distances are propagated throughout, but they are excluded from the figure because they are systematic.

In Figure 6, the dotted curve adjacent to the SED for the YSO in Holoea is the synthetic broadband SED for a K2 giant obscured in its immediate vicinity by normal dust with an optical depth of 0.72 mag at 1 μm. The observed SED displays a large near-infrared excess, with $V-K_s$ being 1.9 mag too red.

In the optical and near-infrared, the SED for the YSOs in MB 4 most closely resembles that of an unobscured M1 giant. For the northern member of the pair, $V-I$, $V-J$, and $V-H$ are all within about 0.1 mag of the colors of the giant. However, there is an excess at K_s, with $V-K_s$ being 0.6 mag too red. If instead the spectral types of the stars were similar to that of the YSO in Holoea, then there would have to be a significant amount of local dust to account for the observed value of $V-I$. Based on the average value of $E(V-I)$, the optical depth of the dust would have to be $\tau_1 = 0.46$. The correspondingly reddened SED of a K2 giant is displayed in Figure 6 just below that of the M1 giant. With respect to this star, the $V-K_s$ excess for the northern component is 0.8 mag, higher than for the unobscured giant, but nevertheless reasonable considering what is observed for the YSO in Holoea.

The two components of IRAS 04261+6339 are quite similar photometrically, with the redder star being dimmer (by 0.5 mag in V). The differences cannot be due entirely to differential extinction, because the discrepancy in V magnitudes is 4 times higher than can be explained by the difference in $V-I$ colors. Rather, it is likely that the southern component is intrinsically fainter and cooler than the northern one.

Overall, the SEDs for the YSOs in MB 4 are very similar in shape to that of the YSO in Holoea in both the optical/near-infrared and the far-infrared. How they differ is in the transition between the near-infrared and far-infrared. Considering that two stars contribute to the light of IRAS 04261+6339, *IRAS* luminosities are the same within errors. However, in V, the YSOs in MB 4 are 4 mag brighter, of which only half a mag can be due to the multiplicity. Two mag more are attributable to the dust in the immediate vicinity of Holoea, based on $E(V-I)$ for K2 III, but only if the YSOs in MB 4 are not also heavily obscured by localized dust. Thus, it appears that the far-infrared luminosity does not scale with the intrinsic optical luminosity.

Much of the discrepancy could be due to the tails. *IRAS* measurements are of such low spatial resolution that emission from the tails is included in fluxes. However, care was taken by Magnier et al. (1999a) to exclude the tail from measurements

of optical and near-infrared magnitudes of the YSO in Holoea, and the tail in MB 4 is so faint that contamination of optical and near-infrared photometry can be regarded as negligible. Relative to the starlight, the tail of Holoea is much brighter than that in MB 4, so it is reasonable to suppose that it has a much more significant impact on the far-infrared fluxes. Thus, it is likely that the far-infrared portion of the SED of the YSO in Holoea is actually fainter than that of the SED for the YSOs in MB 4.

6.2. *The Nebula*

Since there is no hint of ionized gas across MB 4, one might hypothesize that the object is a reflection nebula. Indeed, the $V-I$ color of MB 4 is 0.50 ± 0.20 mag bluer than that of the combined color of the two YSOs near its center. However, the apparent magnitude in I is 1.57 ± 0.17 mag brighter than that of the stars. For MB 4 to be a reflection nebula, the stars would have to be differentially extinguished by at least 1.6 mag, presumably by dust in their immediate vicinity. Such heavy obscuration would be accompanied by a color excess of at least $E(V-I) = 1.2$ mag if the dust is similar to that in the diffuse interstellar medium. In turn, this would require that the differentially corrected $V-I$ color of the stars be less than 0.6, namely at least 0.7 mag bluer than that of MB 4. Thus, it is improbable that MB 4 is a traditional reflection nebula.

MB 4 cannot be a light echo, either. In 1995.9, the nebula appeared 13 lt-yr across at its greatest extent. Yet, the brightest features discernible on the blue and red POSS-II images, which were acquired in 1993.8 and 1993.9, respectively, are coincident in position with the brightest parts visible in V and I fully 2 yr later.

What is notable about MB 4 is its brightness at I compared to bluer or redder bandpasses. This suggests that the mechanism powering the nebula is similar to that behind extended red emission regions (EREs), such as the Red Rectangle (Cohen et al. 1975; Witt et al. 1998), for which the spectrum of emission is observed to peak between 6000 and 8500 Å with a full width at half-maximum ranging from 1200 to 2100 Å . Even though they were first found in association with evolved stars, EREs are now known to be ubiquitous and have been recognized even in the diffuse interstellar medium (Gordon et al. 1998). Recent laboratory work by Ledoux et al. (2001) has produced compelling evidence that photoluminescence of silicon nanoparticles is responsible and readily attributes variations in the wavelength of peak emission to differences in the average size of the particles. If silicon nanoparticles are behind the glow of MB 4, then the brightness in I relative to V indicates that the average size must be at the large end of the range over which photoluminescence is efficient. Given how cool the YSOs appear to be, an alternative source of mid-ultraviolet photons, such as an accretion disk, would have to be present to power the emission. So far, no large-scale nebulosity has been found to be associated with Holoea.

Remarkably, the tails in MB 4 and Holoea have the same physical length in H. Also, the morphology of the tails shifts with wavelength in a comparable fashion, in that they appear more diffuse at longer wavelengths (see Magnier et al. 1999a). However, the tail in MB 4 is only visible clearly in the near-infrared, whereas that of Holoea is also readily observable in the optical. There is only marginal evidence for Hα emission in the tail in MB 4, whereas the tail of Holoea is bright in Hα. Magnier et al. (1996, 1999a) consider the tail of Holoea to be a reflection nebula, so the visibility and morphology are sensitive to the details of how dust is distributed between the source of illumination and the scattering medium.

It might be surmised that the plume in MB 4 is a consequence of a jet at the end of the Class I phase of evolution of one of the two embedded YSOs. There is no counterplume visible, but given the orientation of the observed plume with respect to the filament of dust and gas at the edge of which IRAS 04261+6339 is situated, any counterjet would have been directed into low-density material. Any remaining signature may simply be too faint to see.

Neither Holoea nor MB 4 exhibit a countertail, although Holoea exhibits kinematical evidence for a bipolar outflow. Notably, the tail in MB 4 is pointed 66° away from the plume. If the plume arose from a jet, then it is possible that the misalignment is a consequence of precession. Alternatively, this may be evidence that the southern YSO, which has no associated tail, was the origin of the outflow.

One possible explanation for the disk of MB 4 is that it is a nebula akin to a "blister" on the side of a molecular cloud. As shown earlier, IRAS 04261+6339 is located at the edge of a filament of dust and gas. Suppose that there were an outflow in the form of a jet and counterjet from one of the stars. If there were a sharp enough transition between the cloud and intercloud medium, then it is conceivable that the drop in pressure would have caused the material entrained in the counterjet to spread out across the interface. In other words, the disk would define the place where the counterjet burst out from the cloud. IRAS 04261+6339 would appear offset from the center, as observed, because the counterjet would have emerged from the cloud at a place different from where it originated.

It is also possible that the disk component is a result of the binary nature of IRAS 04261+6339. If the activity of one star were accompanied by ejection of material close to the orbital plane of the pair, then some of the ejecta might have been gravitationally focused as the companion moved through it. Then, a disklike geometry could have been imposed on the outflow, as happens with novae (Hutchings 1972). It is also possible that such an ejection would have exposed the other star if the ejecta were able to push the extremities of its accretion disk away.

For the binary hypothesis to be tenable, the orbital timescale would have to be comparable to or shorter than the time required for ejecta to travel from one component of the binary to the other. Given the angular separation of the stars (Table 1) and the distance, the orbital period must be at least 700,000 yr if the stars have masses of $\sim 1\ M_{\odot}$, or 10 times less if the stars are 10 times heavier. For ejecta to traverse the system in one orbital period or longer, it would have had to move more slowly than 0.1 km s^{-1} in the first case and 1 km s^{-1} in the second. In other words, the velocity of the ejecta would have had to have been very low. The only way that more rapid ejection would be allowable (to explain the disk of MB 4) would be if the active YSO were itself a binary with a shorter period. As yet, no such system has been resolved.

Expanding at 1 km s^{-1}, the time required for the disk to reach its present size would have been 2 Myr. Thus, if ejection were soon followed by the exposure of the stars, then one would expect that the visibility of the YSOs on the POSS would be much as it is today. Indeed, both are readily visible on the 103aO image of the POSS-I[16] (epoch B1954.98), with the photographic B magnitudes being 17.55 and 17.77 for the northern and southern component, respectively (Monet et al. 2003). On the IIIaJ image of the POSS-II (epoch 1993.78),

[16] The National Geographic Society–Palomar Observatory Sky Atlas (POSS-I) was made by the California Institute of Technology with grants from the National Geographic Society.

photographic *B* magnitudes are 17.76 and 17.81, respectively (Monet et al. 2003). The separate results are consistent within errors, suggesting no significant variability.

If indeed the disk of MB 4 were created by binary action, then its plane ought to be aligned with the orbital plane of the YSOs. Approximating the disk as thin, the axis ratio for the inner disk suggests a tilt of 68° to the line of sight. The fact that the axis of the plume deviates from the minor axis of the disk implies that the direction of collimated ejection could not have been perpendicular to the orbital plane.

7. CONCLUSIONS

A large nebula of low surface brightness has been discovered in wide-field *V* and *I* images of the dwarf galaxy UGCA 92 in the constellation Camelopardalis. It is most prominent in *I*, with the morphology of an inclined disk 6′.8 (4.0 pc) across with an emerging jetlike plume 3′.8 (2.2 pc) long. Offset by 30″ from the center of the disk and by perhaps half as much from the base of the plume is IRAS 04261+6339, which *IRAS* colors and spectra reveal to be a widely separated pair of YSOs residing in the Perseus Arm. The northern member exhibits a tail on 2MASS images, the length of which is 15″ (0.15 pc) in *H*. In Hα, the stars are readily visible, but the nebula is not, and there is only marginal evidence for the tail. No H I has been detected at extragalactic velocities. It is concluded that the nebula is associated with the YSOs.

Based on published maps of the Milky Way at 100 μm and in ^{12}CO, the nebula is located near the end of a long filament of dust and gas. The disk is tangential to the edge of the filament, and the plume is directed inward along a direction close to that of the maximum gradient in density. Any counterplume would be projected into a medium of lower density and so may be invisible as a consequence. The tail of the northern YSO is pointed 66° away from the axis of the plume.

Based on *IRAS* colors, the YSOs appear to be transitional objects like IRAS 05327+3404, the central star of Holoea. Although the YSOs in MB 4 and Holoea have comparable far-infrared luminosities, those in MB 4 appear to be brighter in the optical/near-infrared, even after accounting for differential obscuration by localized dust. It is likely that far-infrared fluxes for the YSO in Holoea are biased by emission from the tail, which in the optical/near-infrared is much brighter relative to direct starlight than it is in MB 4. Neither YSO in MB 4 appears to have varied significantly since the 1950s.

The brightness and color of the nebula relative to the YSOs appear to rule out reflection as the source of light. The positional stability of the brightest features suggests that the nebula is not a light echo either. Its brightness in *I* compared to other bandpasses suggests that the glow is caused by photoluminescence of silicon nanoparticles.

The plume may be a remnant of a past jetlike ejection from one of the YSOs. It is possible that the disk component is akin to a blister, having developed as a result of the emergence of a counterjet from the molecular cloud. Alternatively, the disk might be a consequence of gravitational focusing by one star as matter was ejected by the other. If so, then the lower limit to the period of the orbit requires that ejecta have been moving slower than about 1 km s^{-1}. Given the size of the disk today, this places the ejection event at least 2 Myr in the past.

Since there appears to be very little ionized gas associated with MB 4, it is likely that the bulk of the nebula is molecular. Thus, observations of CO emission should be particularly valuable in further elucidating the structure and kinematics of this intriguing object. If nanocrystalline silicon is indeed behind the nebula's visibility, then it may be productive to search for evidence of past outflows around other YSOs by imaging deeply in *I*.

Thanks are conveyed to the staff of Kitt Peak National Observatory for their assistance. M. L. M. thanks the Natural Science and Engineering Research Council of Canada for its continuing support. R. J. B. acknowledges the support of NSF EPSCoR grant RII8996152. This research has made use of the NASA/IPAC Extragalactic Database (NED), which is operated by the Jet Propulsion Laboratory, California Institute of Technology, under contract with the National Aeronautics and Space Administration.

REFERENCES

Bessell, M. S. 1990, PASP, 102, 1181
Bohlin, R. C., Savage, B. D., & Drake, J. F. 1978, ApJ, 224, 132
Burton, W. B., & Hartmann, D. 1994, Ap&SS, 217, 189
Buta, R. J., & McCall, M. L. 1999, ApJS, 124, 33
Carpenter, J. M. 2001, AJ, 121, 2851
Cohen, M., et al. 1975, ApJ, 196, 179
Cutri, R. M., et al. 2003, Explanatory Supplement to the 2MASS All Sky Data Release, http://www.ipac.caltech.edu/2mass/releases/allsky/doc/explsup.html
Dame, T. M., Hartmann, D., & Thaddeus, P. 2001, ApJ, 547, 792
Dame, T. M., Ungerechts, H., Cohen, R. S., de Geus, E. J., Grenier, I. A., May, J., Murphy, D. C., Nyman, L.-A., & Thaddeus, P. 1987, ApJ, 322, 706
Fitzpatrick, E. L. 1999, PASP, 111, 63
Foster, T., & Routledge, D. 2002, in ASP Conf. Ser. 276, Seeing Through the Dust: The Detection of H I and the Exploration of the ISM in Galaxies, ed. A. R. Taylor, T. L. Landecker, & A. G. Willis (San Francisco: ASP), 123
Gordon, K. D., Witt, A. N., & Friedmann, B. C. 1998, ApJ, 498, 522
Gregory, P. C., & Condon, J. J. 1991, ApJS, 75, 1011
Hales, S. E. G., Masson, C. R., Warner, P. J., Baldwin, J. E., & Green, D. A. 1993, MNRAS, 262, 1057
Hawarden, T. G., Leggett, S. K., Letawsky, M. B., Ballantyne, D. R., & Casali, M. M. 2001, MNRAS, 325, 563
Helou, G., & Walker, D. W. 1988, *Infrared Astronomical Satellite* (*IRAS*) Catalogs and Atlases, Vol. 7: The Small Scale Structure Catalog (NASA RP-1190; Washington: GPO)
Herbig, G. H., & Bell, K. R. 1988, Lick Obs. Bull., 1111
Hodapp, K.-W. 1994, ApJS, 94, 615
Huchtmeier, W. K., Lercher, G., Seeberger, R., Saurer, W., & Weinberger, R. 1995, A&A, 293, L33
Hutchings, J. B. 1972, MNRAS, 158, 177
Ivezić, Z., & Elitzur, M. 2000, ApJ, 534, L93
Kwok, S. 2000, The Origin and Evolution of Planetary Nebulae (Cambridge: Cambridge Univ. Press)
Lada, C. 1988, in Formation and Evolution of Low-Mass Stars, ed. A. K. Dupree & M. T. V. T. Lago (NATO ASI Ser. C, 232; Dordrecht: Kluwer), 93
Landolt, A. U. 1992, AJ, 104, 340
Ledoux, G., Guillois, O., Huisken, F., Kohn, B., Porterat, D., & Reynaud, C. 2001, A&A, 377, 707
Magnier, E. A., Waters, L. B. F. M., Groot, P. J., van den Ancker, M. E., Kuan, Y.-J., & Martin, E. L. 1999a, A&A, 346, 441
Magnier, E. A., Waters, L. B. F. M., Kuan, Y.-J., Chu, Y.-H., Taylor, A. R., Matthews, H. E., & Martin, E. L. 1996, A&A, 305, 936
Magnier, E. A., Volp, A. W., Laan, K., van den Ancker, M. E., & Waters, L. B. F. M. 1999b, A&A, 352, 228
McCall, M. L. 2004, AJ, submitted
McCall, M. L., & Armour, M.-H. 2000, in ASP Conf. Ser. 218, Mapping the Hidden Universe: The Universe Behind the Milky Way–The Universe in H I, ed. R. C. Kraan-Korteweg, P. A. Henning, & H. Andernach (San Francisco: ASP), 1
McCall, M. L., & Buta, R. J. 1995, AJ, 109, 2460
———. 1997, AJ, 113, 981

McCall, M. L., Buta, R. J., & Huchtmeier, W. K. 1995, IAU Circ., 6159, 1
McGlynn, T., Scollick, K., & White, N. 1998, in IAU Symp. 179, New Horizons from Multi-Wavelength Sky Surveys, ed. B. J. McLean, D. A. Golombek, J. J. E. Hayes, & H. E. Payne (Dordrecht: Kluwer), 465
Monet, D., et al. 2003, AJ, 125, 984
Moshir, M., et al. 1990, *IRAS* Faint Source Catalog, Version 2.0 (Greenbelt: NASA GSFC)
Ochsenbein, F., Bauer, P., & Marcout, J. 2000, A&AS, 143, 23
Pickles, A. J. 1998, PASP, 110, 863
Reid, M. J. 1993, ARA&A, 31, 345
Reipurth, B. 1994, A General Catalogue of Herbig-Haro Objects (Boulder: CASA), http://casa.colorado.edu/hhcat
Sanner, J., Altmann, M., Brunzendorf, J., & Geffert, M. 2000, A&A, 357, 471
Strauss, M. A., Huchra, J. P., Davis, M., Yahil, A., Fisher, K. B., & Tonry, J. 1992, ApJS, 83, 29
Strong, A. W., & Mattox, J. R. 1996, A&A, 308, L21
Wheaton, W. 2000, in 2MASS Second Release Explanatory Supplement (Pasadena: Caltech), http://spider.ipac.caltech.edu/staff/waw/2mass/opt_cal/#s19
Wheelock, S. L., et al. 1994, *IRAS* Sky Survey Atlas: Explanatory Supplement (JPL 94-11; Pasadena: JPL)
Witt, A. N., Gordon, K. D., & Furton, D. G. 1998, ApJ, 501, L111